Journal of Atmospheric and Solar–Terrestrial Physics 220 (2021) 105626

Contents lists available at ScienceDirect

Journal of Atmospheric and Solar-Terrestrial Physics

journal homepage: www.elsevier.com/locate/jastp

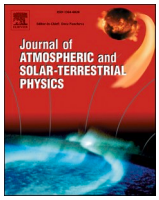

How does the magnetosphere go to sleep?

T. Moretto [a,*,1], M. Hesse [b], M. Kuznetsova [c], L. Rastätter [c], S. Vennerstrøm [d], P. Tenfjord [a]

[a] University of Bergen, Norway
[b] NASA Ames Research Center, USA
[c] NASA Goddard Space Flight Center, USA
[d] Danish Technical University, Denmark

A B S T R A C T

Energy and circulation in the Earth's magnetosphere and ionosphere are largely determined by conditions in the solar wind and interplanetary magnetic field. When the driving from the solar wind is turned off (to a minimum), we expect the activity to die down but exactly how this happens is not known. A recent study utilized global MHD simulations to addressed the questions of what constitutes the quietest state for the magnetosphere and how it is approached following a northward turning in the IMF that minimizes the driving. An exponential decay with a decay time of about 1 h was observed in several integrated parameters related to different aspects of magnetospheric activity, including the total field-aligned current into and out of the ionosphere. The same time rate of change for the cessation of activity has also been measured in total field aligned current estimates from the AMPERE project, adding observational support to this finding. The observational study also revealed both a seasonal and a day/night variation in the decay parameter, with faster decay observed in the winter than in the summer hemisphere and on the nightside than on the dayside. Decay time averages varied between 0.8 and 2.0 h for these scenarios. The results can be understood in terms of stronger/weaker line tying of the ionospheric foot points of magnetospheric field lines for higher/lower conductivity. Additional global modeling results with varying conductance scenarios for the ionosphere confirm this interpretation and provide a quantitative understanding of the effect.

1. Introduction

As first suggested by Dungey (1961), plasma circulation and energization in the magnetosphere are powered by magnetic reconnection taking place at the dayside magnetopause and in the tail plasma sheet, respectively. Most major advancements in magnetosphere research made since then, relate to the verification and details in the implementation of this concept of the open magnetosphere (see, for example, Southwood et al., 2015; Lockwood, 2016, and references therein). Perhaps quite naturally, the bulk of this research has focused on different modes of magnetospheric dynamics, namely how the magnetosphere and its various components evolve over time associated particularly with the response to variations in the direction of the interplanetary magnetic field (IMF). A complete review of this huge body of work is outside the scope of this report. Some key observational works include: Nishida (1968); Friis-Christensen et al., 1985; Ridley et al. (1998); Murr and Hughes (2001); Lu et al. (2002); Ruohoniemi et al. (2002); Fiori et al. (2012); Grocott and Milan (2014); Dods et al. (2017); Snekvik et al. (2017); Anderson et al. (2018); McPherron et al. (2018), Milan et al. (2018), and references herein. The vast variety of different aspects of the dynamics, from substorms to geomagnetic storms, plasmoid formation and ejection, formation and evolution of ring current and radiation belts, coupling to the ionosphere and relation to auroral features, has understandably formed tantalizing research targets and continues to do so today.

In comparison, the quiet magnetosphere, by which is understood a magnetosphere devoid of major energization and dynamical changes, has received only little attention. Its existence is often implicitly assumed. A prominent example is in the establishing of base-lines for observations of ionospheric and geomagnetic parameters, including geomagnetic indices (for a recent list and descriptions see, e.g., Kauristie et al., 2017). Traditionally, the derivation of base-lines (also often termed quiet day curves) has built on the concept of quiet days (e.g. Campbell, 1989; van de Kamp, 2013) but recently statistical analysis approaches have also been successfully developed and employed (e.g. Gjerloev, 2012; Klausner et al., 2016). A practical implication of the identification of the quiet magnetosphere and associated geomagnetic sources is for modeling of the Earth main field. A recent overview of the various approaches and models currently being employed is provided in Finlay et al. (2017).

The quiet magnetosphere is often conjectured to result from certain solar wind conditions, which would minimize the driving at the

* Corresponding author. University of Bergen, Norway.
E-mail address: Therese.m.jorgensen@nasa.gov (T. Moretto).
[1] Full name: Therese Moretto Jorgensen.

https://doi.org/10.1016/j.jastp.2021.105626
Received 1 June 2020; Received in revised form 7 January 2021; Accepted 18 March 2021
Available online 26 March 2021
1364-6826/

magnetopause, such as northward IMF orientation, small magnetic field magnitude, and low solar wind density and velocity. The most likely combination of parameters to achieve the quiet state can be deduced from solar wind-magnetosphere coupling functions, of which quite a few exist (see, for example, Akasofu, 1981; Gonzalez, 1990; Newell et al., 2007; Borovsky, 2008; Milan et al., 2012; and Tenfjord and Østgaard, 2013, and references herein). It should be noted, however, that the coupling functions present a complementary but not independent aspect of the quiet magnetosphere as they all are derived and verified based on geomagnetic indices.

While the existence of the quiet magnetosphere is widely accepted on a conceptual level and useful from the point of view of developing static, theoretical models, its existence on a more fundamental level is poorly understood. Very little work has been devoted to the question of what the precise nature of the quiet magnetosphere is, how long the system takes to reach such a state, and, ultimately, whether such a state even exists uniquely. The aim here is to review and describe some current studies pertaining to these questions. First, in Section 2, we describe a recent study utilizing global MHD modeling to address the questions of what constitutes a quiet state for the magnetosphere and how it is approached following a northward turning in the IMF that minimizes the driving. Next, in Section 3, we discuss observational evidence for the generic relaxation time-scale for magnetospheric activity that is predicted by the model, including recent results based on observations from the AMPERE project. In Section 4 we return to the model to investigate and quantify the dependence on ionospheric conductance of the relaxation rate that the observations show. Finally, Section 5 presents our conclusions.

2. The quiet magnetosphere in global MHD

Preliminary results from a study of the quiet magnetosphere using global MHD simulations were presented by Hesse et al. (2017). In this section we describe in more detail this study and the results obtained.

2.1. Model and approach

Four different global MHD runs were conducted with the objective to investigate to which degree a relaxed state of the magnetosphere depends on prior history. All simulations were initiated with solar wind conditions, which drive significant activity; however, the IMF was southward for two runs and eastward for two others. In addition, two different solar wind densities were used for further variety of solar wind input conditions. Each run was subjected to its respective driving conditions for 2 h, after which the IMF was turned northward, the solar wind speed was reduced, and the density was set to a common, lower value. After a further 2 h, the latter conditions were augmented by random solar wind fluctuations – identical for all runs, with amplitudes commensurate with typical solar wind observations. The objective for this final phase of the runs was to investigate the nature of quiet magnetospheric states, addressing the question of how quiet a magnetosphere can be in the presence of typical solar wind fluctuations.

The global MHD model employed was a magnetospheric implementation of the Space Weather Modeling Framework (SWMF), version v20140611 (Tóth et al., 2005, 2012). Runs were executed at the Community Coordinated Modeling Center (CCMC) and tailored to the research task: an ultra-high-resolution grid was used with 25 million cells and minimum resolution close to the inner boundary at $2.5R_E$ of 0.0625 R_E together with a low diffusion, so-called Sokolov scheme. The dipole tilt was fixed at near-equinox conditions (March 20, 2015) and not updated for the duration of the run. For the ionospheric solver, an auroral conductance model was used to represent conductance variations due to diffuse and auroral particle precipitation, as well as due to solar ultra-violet flux.

The solar wind conditions were applied in three separate phases. During the first 2 h, conditions commonly associated with a driven, active magnetosphere were applied. These conditions differed between the runs that were conducted. After 2 h, for all runs, the IMF was changed to purely northward ($B_z = 5$ nT), the density to 5 cm^{-3} and the solar wind speed reduced to 300 km/s for another 2 h. This set of parameters is chosen to minimize the expected energization of the magnetosphere from the combined effects of viscous interaction with the solar wind as well as merging with the northward IMF tail-ward of the cusp (Bhattarai et al., 2012). Finally, for the last 2 h, to all key parameters was added a 10% fluctuation level (that is, with amplitudes of 0.5 nT for B_z and B_z, to 0.5 cm^{-3} for the density, 30 km/s for each of the velocity components, and 2.4×10^4 K for the temperature), which is not uncommon for the solar wind. While the fluctuations were entirely random, they were the same for all runs conducted. The IMF B_x is set to zero for the entire simulation period.

One of the key questions in investigation the relaxation of a previously active magnetosphere to a quiet state, is how much the latter, as well as the relaxation time, depend on the prior, active state. In order to shed light on this question, four different simulations were conducted, each featuring different solar wind conditions during the first 2 h. In run 1, an IMF $B_y = 0$ nT and $B_z = -5$nT, a density of $n = 5$ cm^{-3}, and a solar wind speed of 500 km/s were applied. Conditions for run 2 were identical, except that the density was increased to 10 cm^{-3}. The solar wind conditions for runs 3 and 4 replaced the IMF conditions of runs 1 and 2, respectively, with IMF conditions of $B_y = 5$ nT and $B_z = 0$ nT. As illustration, the full solar wind inputs, including the parameters not discussed here, are displayed for runs 1 and 4 in Fig. 1.

3. Results

Results of run 1 are presented here in detail and an overview of key results from run 4 is also given. Results from the other runs are included for comparison but not discussed in detail. First for an overview of the simulation output, Fig. 2 displays a meridional cut at $y = 0$ of the magnetic field, flow vectors, and pressure for run 1. The three panels (from top to bottom on the left) are plotted at the end of the three solar wind driver phases, at time ~2 h, 4 h, and 6 h into the simulation. The top left panel shows a typical active magnetosphere, with indications of both dayside and tail reconnection. The magnetosphere is considerably more relaxed in the middle left panel (at time 4 h), with an outwardly expanded magnetopause and a much wider region of closed magnetic field (magnetic field lines connected to the earth at both ends). The growth of the closed field line region appears to continue also through the last 2 h (bottom left panel), seemingly indicating that the magnetosphere continues to relax. The analysis below will show that this impression is misleading, though.

Exhibited in Fig. 2 (panels on the right) are also results for the ionosphere, namely field-aligned current patterns in color, contours of the polar cap potential, and the open-closed field line boundary, at the same times as for the magnetosphere panels on the left. Only the northern ionosphere is shown here. The results for the southern ionosphere are practically identical, as expected for near-equinox conditions and purely IMF B_z driving. Corresponding to the magnetosphere depicted in the top left panel, the ionosphere in the top right panel shows a typical active signature, with a large open field-line region, surrounded by region 1 type current patterns. Despite the absence of an inner magnetospheric model in these simulations, the results also feature weak region 2 type currents at lower latitudes. The situation is entirely different in the middle and bottom panels on the right, where we find highly reduced currents and potential values, and a minimal open field line region. We note, however, that the latter may well be underrepresented in global MHD models (Rastätter et al., 2005; Anderson et al., 2017). Clearly depicted in these panels, above 80° magnetic latitude, are the so-called NBZ currents (Iijima et al., 1984) and corresponding reversed convection cell potential pattern associated with reconnection between the IMF and magnetosphere fields taking place tail-ward of the cusp as expected for northward IMF conditions (e.

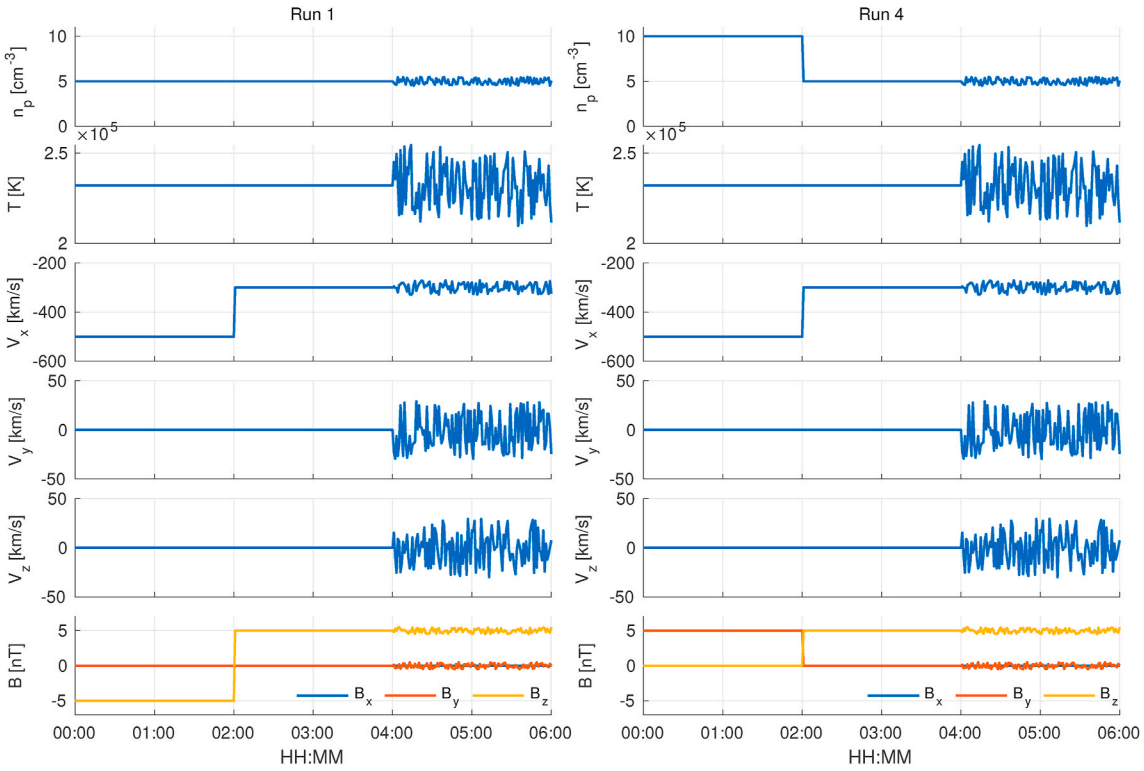

Fig. 1. Depicted is the solar wind input used in simulation runs 1 (left) and 4 (right). From top to bottom are shown the ion density, the temperature, three components (GSM X, Y, and Z) of the velocity, and the vector components (GSM X, Y, and Z) of the magnetic field.

g. Crooker, 1992; Vennerstrom et al., 2005). Also clearly present in the middle panel at magnetic latitudes between 70 and 80° is a set of weaker convection cells and corresponding field-aligned currents of opposite polarity, presumably the result of viscous interaction between the solar wind and magnetosphere, which completes the typical four-cell pattern expected for northward IMF conditions (e.g. Burke et al., 1979; Vennerstrom et al., 2005). Again, very little difference is observed between the middle and bottom panels.

It is possible to capture the overall state of the magnetosphere and its evolution by studying certain integrated parameters. To this end, integrated values for the currents into or out of the model ionosphere, the ionospheric potential, and, for verification purposes, the ionospheric Joule dissipation were investigated. The results for run 1 (panels on the left) and run 4 (panels on the right) are shown in Fig. 3. Time is counted in hours centered on the northward turning of the IMF that took place 2 h into each run. The two runs exhibit essentially identical evolutions in these parameters and the evolution is also virtually identical between hemispheres for all parameters. During the first hour, we see an adjustment of the model to the driving conditions and subsequent steady driving for the second hour. The amplitudes of all parameters exhibit an overshoot in response to the northward turning and then reduce rapidly during the following 2 h. During the final 2 h the effects of adding the fluctuations to the solar wind driving are observed to be to induce large, similar fluctuations in all parameters.

As indicated in the figure, in all cases the decay phase during the middle 2 h is exceptionally well represented by an exponential decay $\sim \exp(-\lambda t)$. For the time constant (e-folding time, $t_0 = 1/\lambda$), we find the following values for the electric potential ($\Delta\phi$): $t_{0,\phi}\sim$1 h, for the integrated current (J): $t_{0,j}\sim$0.9 h, and for the Joule dissipation: $t_{0,W}\sim$0.5 h. Remarkably, the same e-folding times are seen in both runs even as the overall amplitude of the parameters in run 4 is about 20% lower than in run 1. This finding indicates that the decay process is following an intrinsic internal time scale, and that it depends on the starting state only to a smaller degree. The faster time decay of the Joule dissipation illustrates the internal consistency between the results. The Joule dissipation can be approximated by $\boldsymbol{W} = \int \boldsymbol{j}_{\parallel}\phi \boldsymbol{dA}$(e.g. Richmond, 2010), where the integral extends over a spherical surface at some suitable altitude above the ionosphere. This relation indicates that the decay times of current, potential, and polar cap potential should be related, with: $1/t_{0,\phi}+1/t_{0,J}\sim 1/t_{0,W}$.

The remaining two runs also exhibit essentially the same behavior in the decay. This is shown in the panels on the left in Fig. 4, which displays the time evolutions of currents and potential for all four runs in a format similar to that of Fig. 3 but only including the northern hemisphere. We find, again, that the driven phase leads to qualitatively similar time evolutions, albeit with higher amplitudes in both currents and potentials for southward IMF primarily (red and magenta curves), and higher solar wind density secondarily (magenta and blue curves). Not only is the decay behavior qualitatively identical, it also, at least to some degree, preserves the amplitude ordering, whereby for example, run 1 maintains a higher current amplitude than run 4 during the decay phase. It appears that the magnetosphere, at least in the model representation here, has generally a typical decay time of 1 h, but retains some memory of its history after 2 h of relaxation under northward IMF and reduced solar wind speed.

]An interesting question is whether exposure to fluctuations in the solar wind driver reduces or eliminates completely the system's memory of the prior history. For the purpose of investigating this question, we applied exactly the same fluctuations to all four runs during the last 2 h. The panels on the righthand side in Fig. 4 display enlargements of the current and potential evolutions of all four runs during the last 3 h of the runs. The effects of the fluctuations are seen in the ionosphere with a delay of about 0.2 h, which match well the expected time it takes for the change to propagate from the upstream boundary of the simulation at 32 Earth radii to the magnetopause and couple through the magnetosphere to the ionosphere (see e.g. Ridley et al., 1998; Milan et al., 2018). We notice two key facts: 1) the fluctuations drown out any further decay that might otherwise have continued in the ionospheric potential and

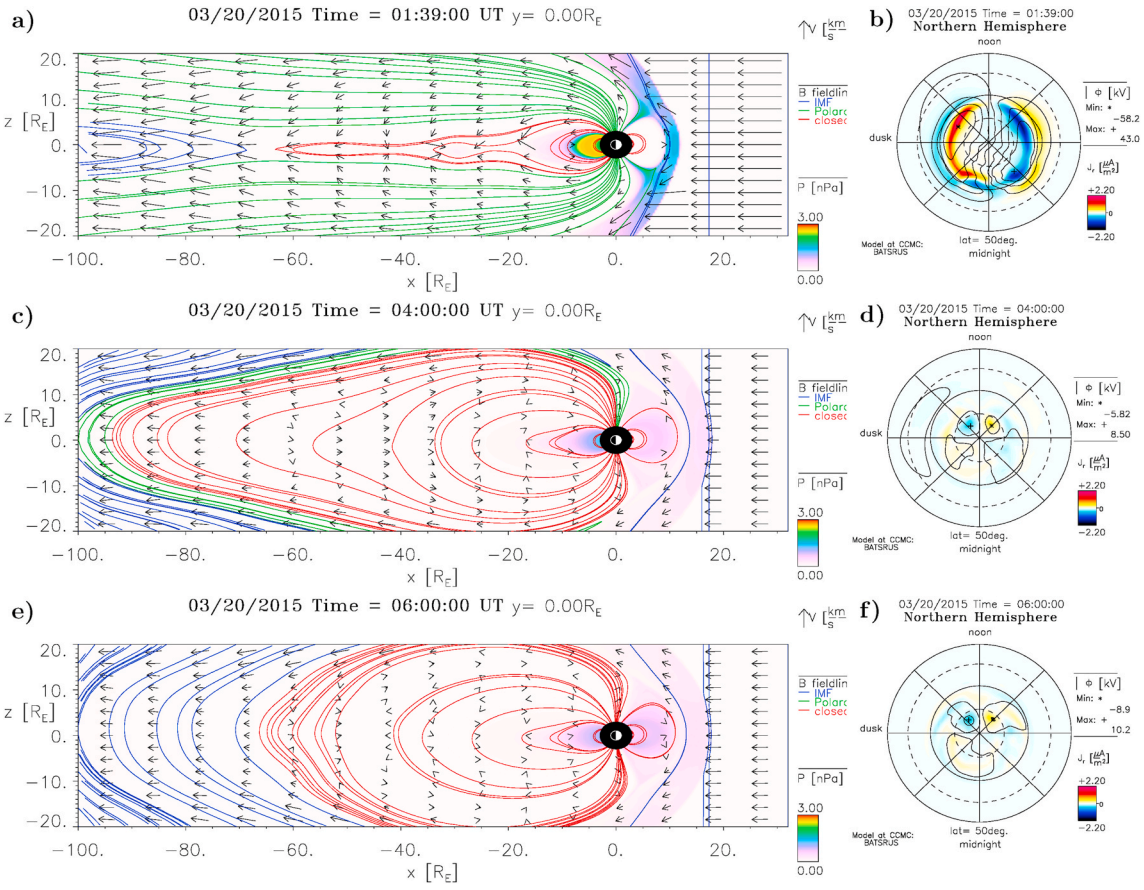

Fig. 2. On the left are shown panels of magnetosphere pressure (color contours), magnetic field lines (blue lines are IMF, black lines are open and red lines are closed) and flow vectors in the noon-midnight plane at three different times (01:30 UT at the top; 04:00 UT in the middle; and 06:00 UT at the bottom). On the right are show corresponding panels (at the same three points in time) of the northern ionosphere (seen from above the north magnetic pole with noon towards the top and the lowest magnetic latitude circle at 50°) field aligned current (color contours) and electric potential (contour lines). Indicated with a thick black line is the position of the boundary between thee open and closed magnetic field.

currents (as well as the dissipation, not shown), leaving the potential to fluctuate at a level of about 30% around roughly15kV, and the currents to fluctuate at a similar level around roughly 0.5 MA; and 2) the time evolutions continue to preserve the amplitude ordering observed 2 h after the northward turning, with run 1 having the largest current, and run 4 the largest potential. While this ordering indicates that the system's memory time is apparently longer than 4 h, it is also apparent that all four runs respond to the applied fluctuations in essentially the same way, with exceptionally high correlations between the traces for both current and potential. System memory is therefore found to be insufficient to dominate the evolution. Instead, the model reacts, in this integrated sense, rather similarly to the driving conditions, irrespective of the prior history.

4. Conclusions

In all four cases examined, not surprisingly, the driven phase establishes a large open magnetic flux region, significant cross polar cap potentials, and current systems, the amplitudes and locations of which depend on the solar wind driver. The relaxation starts with the states attained after 2 h as initial condition. Somewhat surprisingly, we find a very well-defined exponential decay of typical parameters, such as total current flow into or out of the ionosphere. A further surprise is that, independent of the initial condition, the decay time is approximately 1 h for all runs. The main sign of memory of the initial state proves to be that the amplitude ordering at the start of the relaxation, that is, for example, which run features the largest currents, remains throughout the evolution. We suggest that the decay time is related to the expected decay of a twisted flux tube when coupled to a medium of finite conductance, within which the field-aligned currents close. Within this, certainly rather simple, concept, it seems reasonable that larger currents take longer to decay to the same level as a current system of initially lower amplitude.

In summary, these findings indicate that most of the memory of the prior state is lost within about 1 h, which therefore can be seen as a typical transition time between states in response to different driving conditions. The results also suggest that it may be quite difficult to define a proper "quiet state" of the magnetosphere; the main reason being that solar wind fluctuations continue to drive activity, even if the overall driving conditions are minimal (IMF is northward). This effect can be amplified by the nonlinear nature of the driver: for example, the kinetic pressure is proportional to the density and the square of the velocity, so that correlations between fluctuations of individual quantities can have larger impacts. As regards system memory, we find, in addition to the "short term memory" of about 1 h also a "long term memory," which persists through the entire evolution. This memory effect may make it even more difficult to define a single "quiet state." Finally, we point out that this study was based on a single MHD model, albeit of very high resolution and low diffusivity.

5. Observational evidence

Few observational studies exist that address the questions of the nature and emergence of the quiet magnetosphere. In this section we

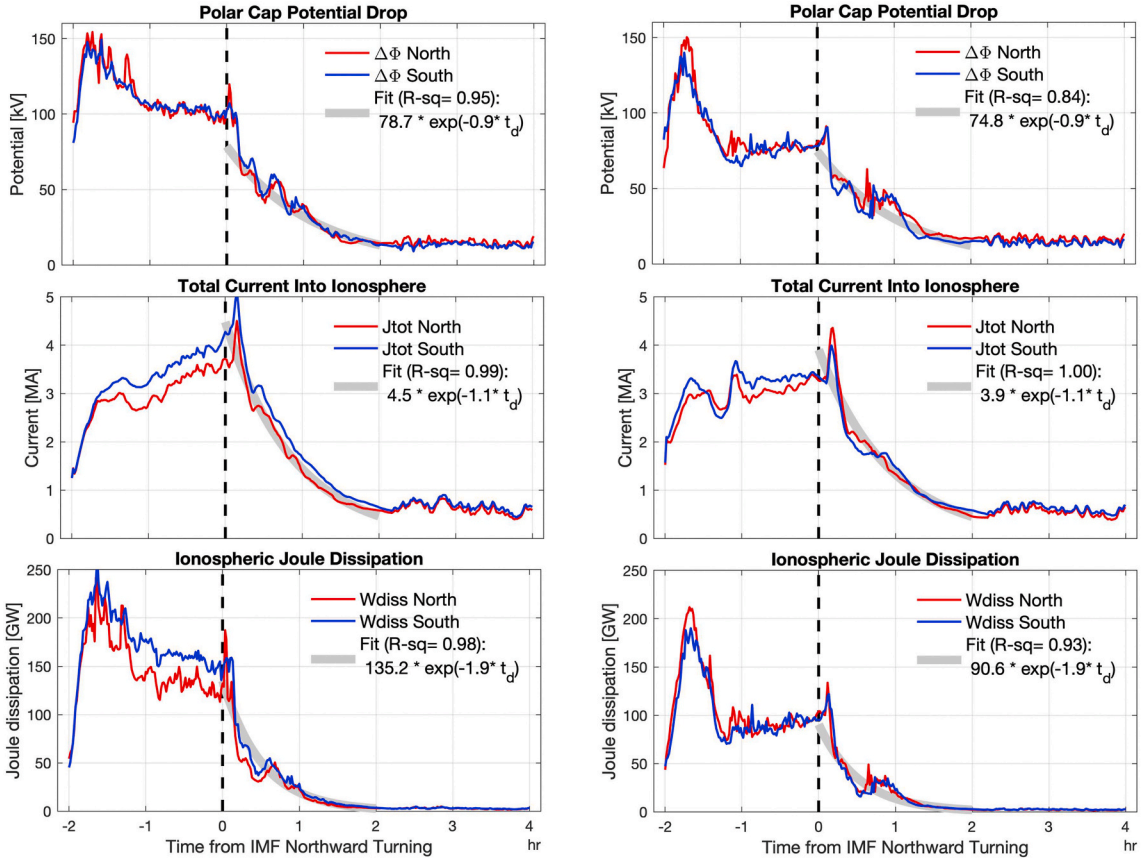

Fig. 3. The panels on the left display the time evolution of the maximum difference in electric potential (top), integrated field-aligned current into the ionosphere (middle), and total Joule heating dissipation (bottom) for the northern (red lines) and southern (red lines) hemispheres for Run 1. Time is counted in hours centered on the time of the northward turning of the IMF. Also shown in each panel (thick light grey line) is an exponential fit to the data (for the northern hemisphere) during the first 2 h after the turning. The parameters for the fits are provided in the legends. The panels on the right show the corresponding results for Run 4.

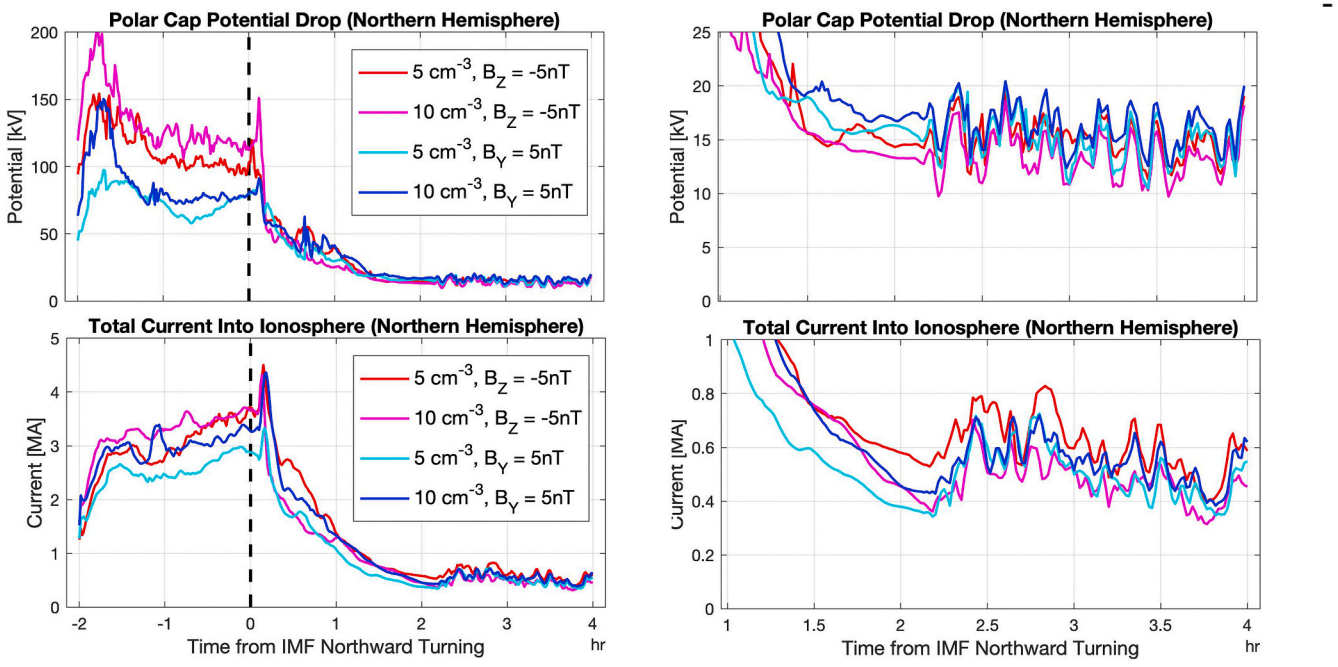

Fig. 4. The panels on the left display the time evolution of the integrated electric potential (top) and field-aligned current into the ionosphere (bottom) for the northern hemisphere for all four runs with colors as indicated in the legend. Time is counted in hours centered on the time of the northward turning of the IMF. The panels on the right provide an expanded view of the same data for the last 3 h of the runs.

describe some relevant earlier studies as well as some recent studies that have been conducted based on newly available observations of global field aligned current distributions.

5.1. Early findings

An early observational indication of magnetospheric memory was provided by Wygant et al. (1983) who reported on the existence of an extended time response in the cross polar cap potential during long periods of northward IMF conditions. Their study compared observed polar cap potential drops from a polar crossing satellite with predictions based on estimates of the dayside reconnection electric field from various combinations of solar wind measurements. They found that introducing a weighted average of solar wind parameters over the preceding 4 h, with a weighting function in the form of an exponential decay with a time scale of 3 h, significantly improved the agreement between the predicted and observed potentials as compared to predictions based on hourly averaged solar wind parameters. They interpreted the existence of this extended time response in their results as the time constant for magnetospheric convection to « turn off » after previous periods of high reconnection rates.

Other earlier studies mainly have been aimed at establishing the time it takes for convection and current systems in the magnetosphere and ionosphere to reorganize from one characteristic pattern to another following a change in IMF. Most studies concern the case of how activity develops and current and convection systems are set up following a change in the IMF from northward to southward. Far fewer studies have presented results specifically for the opposite change from southward to northward IMF conditions. Typical reconfiguration times for ionospheric convection or current systems in the range of 20–40 min have been reported for single individual events (e.g. Clauer and Friis-Christensen, 1988; Knipp et al., 1991; Hairston and Heelis, 1995). Meanwhile, a statistical study by Ridley et al. (1998) found an average reconfiguration time of 13 min with no significant difference observed between north to south and south to north turnings. This result, which was based on ground-based magnetometer measurements, has since been corroborated by radar measurements of ionospheric convection (see, e.g., discussion in Chisham et al., 2007).

5.2. Recent results from AMPERE

The advent in 2010 of the Active Magnetosphere and Planetary Electrodynamics Response Experiment (AMPERE) project have made available continuous global estimates of the field-aligned currents into and out of the high latitude ionosphere (Anderson et al., 2014). The AMPERE measurements constitute an ideal new resource for assessing

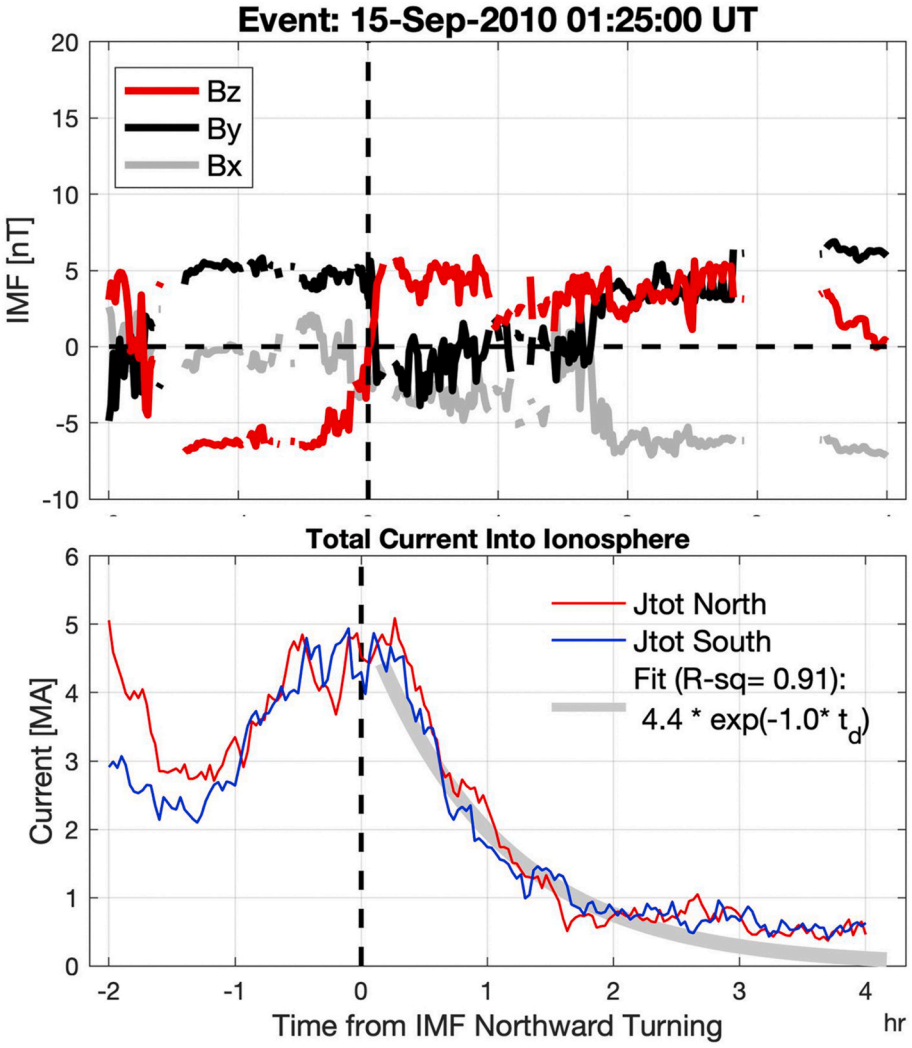

Fig. 5. The IMF (top panel) and total current estimates (bottom panel) from AMPERE for a northward turning example event. The IMF from the OMNI database is shown in GSM coordinates (X,Y, and Z as indicated in the legend). The time is in hours centered on the time of the northward turning observed in the IMF. The format of the figure in the bottom panel is identical to that of Fig. 3.

the evolution of the large-scale convection and current systems in the magnetosphere. Through an extensive analysis of a large set of events identified in the AMPERE dataset, Moretto et al. (2018) was able to directly test and verify the predictions from the global MHD simulations of Hesse et al. (2017) presented in section 2. Events were carefully selected to fulfill the criteria of exhibiting a rapid change from southward to northward IMF, preceded and succeeded by extended periods of steady IMF conditions. An example event is shown in Fig. 5. This event was the one with the longest period of continual northward IMF following the turning (even before the occurrence of the gap in the IMF observations). Displayed are IMF observations together with total currents into the ionosphere measured by AMPERE for both the northern and southern hemispheres in the same format as in Fig. 1 in Moretto et al. (2018). Also indicated in the figure is the fitted exponential decay in the same way as in Fig. 3. A total of 39 such events were identified and analyzed individually and statistically as well as through a superposed epoch analysis. The observational results confirm the characteristic exponential decay for the currents that was seen in the global MHD simulations. The time constant of 0.9 h was also validated in the observational study, measuring a decay constant $\lambda = 0.9$ (± 0.3) h-1 which corresponds to a time constant of 0.8–1.7 h. Further, in agreement with the simulation results, no clear dependence on the amplitude of the current was found for the decay parameter. Rather, the variable that was found to best explain the spread in values for the decay constant was season, with faster decay observed in the winter than in the summer hemisphere. It was concluded that the seasonal variation in ionospheric conductivity independently affect both the amplitude of the current and the decay parameter.

Further evidence for the impact on ionospheric conductivity on the decay rate is found when repeating the analysis of decay parameters conducted in Moretto et al. (2018) separately for nightside and dayside currents. Alongside with the total hemispheric currents, estimates for currents into and out of the nightside and dayside halves of each ionosphere are also provided as a standard product in the AMPERE dataset. For these estimates, dayside is defined simply as the part of the ionosphere between 06 and 18 magnetic local time and, correspondingly, the nightside constitutes the part between 18 and 06. The exponential decay is equally evident in this set of currents and the results of the exponential fitting for all events are shown in Fig. 6. Each panel in the figure corresponds to Fig. 3 in Moretto et al. (2018) but with the analysis done only for the nightside (left panel) or dayside (right panel) part of the currents, respectively. We see that the nightside currents exhibit overall larger values of the decay constant than the dayside set and with much less spread in the values. This behavior matches the expectation that the lower conductivity on the nightside is associated with a faster decay rate. The median value for the time constant (e-folding time) over all nightside currents is $t_{0,j} = 1.0$ h as compared to the median value for all dayside currents of $t_{0,j} = 1.3$ h. Ionospheric conductivity on the nightside also varies much less as a function of season than for the dayside, which may explain the lack of seasonal variation in the decay constant for the nightside. In contrast, the median value for the time constant for the dayside currents exhibits a large difference between the winter solstice events at $t_{0,j} = 0.8$ h and the summer solstice events at $t_{0,j} = 2.0$ h. In summary, we find the fastest decay rate in winter on the dayside and the slowest decay rate in summer on the dayside.

To explain the relation between the decay rate and ionospheric conductivity, consider again what needs to happen for the convection in the magnetosphere to slow down, or stop, namely the unwinding of the field-aligned current carrying flux tubes in the coupled magnetosphere-ionosphere system. In response to magnetic forcing from the magnetosphere conveyed through the JxB force, the ionosphere with higher conductivity (daytime summer conditions) will have a higher resistance to motion thus necessitating a larger current to establish the appropriate magnetosphere-ionosphere coupling. For an ionosphere with low conductivity, in contrast, comparatively little current is needed to establish the coupling. These effects are well documented (e.g Ridley, 2007; Coxon et al., 2016). At the same time, stronger/weaker line-tying in the higher/lower conductivity ionosphere may also explain the longer/-shorter decay time for magnetospheric activity. With low conductivity in the ionosphere and corresponding weaker line-tying of magnetospheric field lines, the unwinding of current-carrying fluxtubes and associated changes in magnetospheric convection that need to happen to reach the new quiet state can be more easily and quickly accomplished (e.g. Coroniti and Kennel, 1973). The opposite is true for the high conductivity case where stronger line-tying makes changes in convection take longer to get established.

The evolution of field-aligned currents in response to changes in the IMF have also been investigated in other studies based on AMPERE data, albeit with very different techniques which make direct comparisons of the results with the decay time scales reported above difficult. Also utilizing the total field-aligned currents on the dayside and nightside, respectively, McPherron et al. (2018) derived linear prediction filters in response to solar wind driving. For both cases, they found response functions with total lengths of 3 h but with different decay shapes, neither of which was seen to exhibit purely exponential decay. The response of the full distribution of the field aligned currents to changes in the IMF was examined by Milan et al. (2018) utilizing a principal component analysis. After northward turnings, the main field-aligned current component (roughly representing the region-1/region-2 current system) on the dayside was seen to decrease over a period of about an hour. However, over the same period of time, a component of the current system roughly corresponding to the dayside NBZ currents was seen to increase to a maximum, implying that the total dayside current would exhibit a slower and more prolonged decay. The decrease

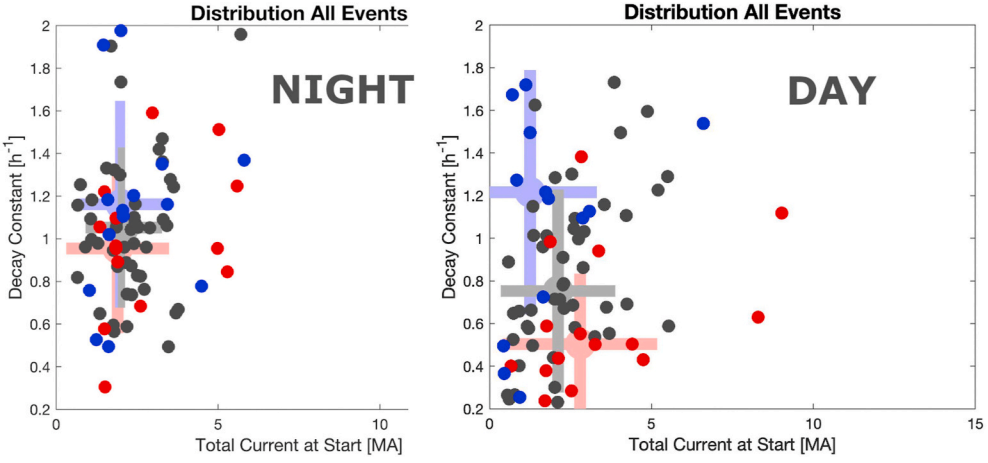

Fig. 6. Scatter plots of fitting parameters derived for the entire ensemble of events and for both northern and southern hemispheres but separately for the nightside parts (left panel) and dayside parts (right panel) of the currents. In each panel, the large, light grey dot and bars indicate the median values and standard deviations for the fitting parameters over the entire dataset. Marked in red are the events around the June solstice and in blue the events around the December solstice with corresponding medians and standard variations (large dots and bars in light red and blue), while the dark grey dots represent events that occur around the equinoxes. The format of the figure in each panel is identical to that of Fig. 3 in Moretto et al. (2018).

observed for the main current component (roughly the region-1/region-2 current system) on the nightside was also much prolonged, reaching a minimum after about 2 h. Further, no indication of effects from substorms were seen in the nightside response in good agreement with the finding that the total current in the substorm current wedge as observed by AMPERE is very small (on the order of 0.1 MA) reported by Clausen et al., 2013. These results also add confidence that the exponential decay constants measured here are not significantly affected by any substorms occurring during the events. The exponential time constant of roughly 1 h measured by Hesse et al. (2017) and Moretto et al. (2018), on the one hand, and the 3-h length of the response filters reported by McPherron et al. (2018) and the 2-h period over which the nightside main current constituents was seen to decrease as reported by Milan et al. (2018), on the other, suggest good overall consistency between the results from these different analysis methods applied to the same AMPERE dataset.

6. Modeling the role of ionospheric conductance

To further investigate the role of ionospheric conductance on the decay rate we return to the global MHD model. In this section we present the results from a series of additional simulations, which were performed to illuminate the role of ionospheric conductance.

6.1. Model and approach

Five additional simulation runs were conducted to investigate the effect of varying the ionospheric conductance in a controlled fashion. The same global MHD model was employed as for the study described in section 2. However, for the purpose of performing just a quick verification of the conductance effect, it was run in a simpler, regular implementation, which implies a somewhat lower resolution and simpler numerical scheme. To facilitate comparison, the solar wind profile used to drive all of the new runs is the one for run 1 of the former set, but without applying the fluctuations to the parameters during the last 2 h. Specifically, the northward IMF conditions were continued uninterrupted for a total of 4 h. The only other simplification made here is that no dipole tilt was included. Only one run used an auroral model for the ionospheric conductance. For the other four runs, to control the ionospheric conductance we followed the approach of Ridley et al. (2004) and apply the simplest ionospheric conductance pattern that will produce a quasi-realistic magnetospheric configuration, namely a uniform zero Hall conductance and a uniform non-zero Pedersen conductance. The four values for Pedersen conductance tested in the runs are: 1, 5,10, and 100mho.

7. Results

The evolution of the integrated field-aligned current into the northern hemisphere is depicted in Fig. 7 for all of five runs. Also depicted in the figure are the exponential fits to the decay observed in the currents for the first 2 h after the northward turning. Contrary to the initial study described in section 2 where the effects of the fluctuations were observed at this point, here the driving wasn't changed. Even so, it is obvious that exponential decay is only a good fit for the first 2 h. That is, these results indicate that even without the added fluctuations the decay changes to a different mode after about 2 h, possibly as the unwinding of the large-scale flux-tubes have progressed to the point that other smaller scale dynamics begin to dominate. As a curiosity we note that the event displayed in Fig. 5, which is one of only a few events in the study for which the IMF remains northward for more than 2 h, exhibits the same behavior. However, fluctuations in the IMF are observed in the event that could also be the cause of this effect. Further investigation of this potential transition in the mode of the decay and the nature of the various processes involved with the global MHD model, including the role of reversed (high latitude reconnection) and viscous convection

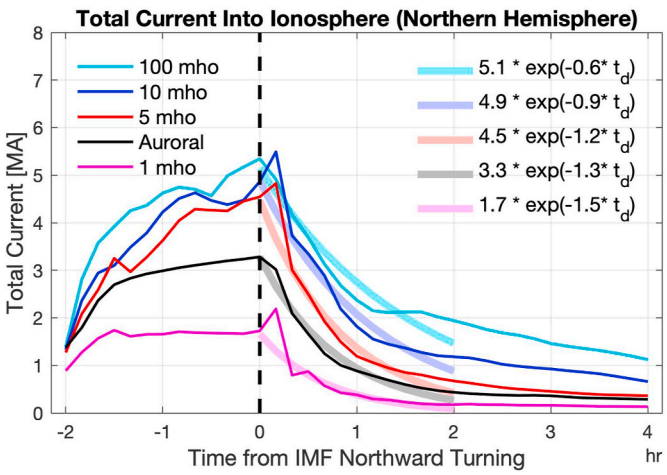

Fig. 7. Time evolution of the integrated field-aligned current into the northern ionosphere for all five runs with colors as indicated in the legend on the left. Time is counted in hours centered on the time of the northward turning of the IMF. Also shown (thick light-colored lines) are the exponential fits to the data during the first 2 h after the turning. The parameters for the fits are provided in the legend on the right.

cells, would be highly interesting. However, such a study would require a new set of purposeful, research-grade simulations and, thus is left for a future effort.

In the comparison between the various runs presented in Fig. 7, the two effects associated with increasing the ionospheric conductance are evident: increased amplitude of the currents during the driving phase and increased time constant for the decay ($t_0 = 1/\lambda$, with λ decreasing). In this behavior, the results fully confirm the expectations based on the observational results and their interpretation in terms of ionospheric conductivity as discussed in section 3. Also noteworthy is the fact that the range of values for λ resulting from this set of conductance values matches well the range yielded by the observational analyses and corresponds to time constants (e-folding times) for the decay roughly between 0.7 and 2 h.

8. Summary and conclusions

New and recent studies are presented, which provide an answer to the question posed in the title: when driving is effectively turned off, magnetospheric activity decays exponentially with a generic time constant of roughly 1 h. This behavior is observed consistently between global MHD simulations and observations of field-aligned currents in the ionosphere. One surprising finding is that the decay rate is independent of the level and nature of the solar wind driving imposed ahead of shutting it off. As an inherent property of the magnetosphere, this behavior may be understood as the expected decay of a twisted flux tube when coupled to a medium of finite conductance, within which the field-aligned currents close. From this idea follows that the decay rate would depend on the level of ionospheric conductance. Higher conductance means stronger line-tying of the magnetic flux tube and more resistance to changing the convection as needed for the flux tube to un-twist. Evidence for this expectation is found in the decay rate for ionospheric field-aligned currents estimated from observations, which exhibit significant variations both with season and between dayside and nightside. Time constants ranging from about 0.8 h for the dayside in winter to 2 h for the dayside in summer are observed. Further direct confirmation of the relation between the decay rate and ionospheric conductance is provided by a set of global MHD simulations done with uniform, constant ionospheric conductance. Varying the conductance from 1mho to 100 mho yields decay constants ranging from 0.7 h to 1.7 h. How the existence of a generic decay rate, independent of the state of the system

at the beginning of the decay, can be reconciled with the expectation within the ideal MHD approximation of entropy conservation for the closed flux tubes is a curious question that warrants further study.

Simulations done with a longer decay phase indicate that the exponential decay only occurs for the first roughly 2 h, after which a near-linear decay at a much slower rate is observed. A few rare events in the field-aligned current observations, for which the IMF remained northward for more than 2 h, seem to support this finding. However, no firm conclusions can be drawn based on the available results so far. Confirming this feature in the decay and revealing the nature of the processes behind it, therefore, is highly recommended as a subject for future studies, but would require additional well-defined advanced model simulations as well as, potentially, additional extensive observational datasets.

On the question of memory in the magnetosphere-ionosphere system, the answer from global MHD model simulations is that after 2 h of relaxation, very little memory remains in the system. Evidence for this result is seen in that all of the runs presented here exhibit a near-identical response, as observed in integrated ionospheric potential and current measures, to fluctuations in the solar wind parameters added after the relaxation phase, irrespective of the level and nature of the driving that is applied prior to the relaxation phase. A small sign of memory, however, is seen in the amplitude ordering of parameters between the simulation runs, most prominently observed in the currents, which is preserved from the start of the relaxation phase through to the end of the fluctuations. The retainment of memory far into the relaxation is bad news for quest to identify and specify a unique quiet (ground) state for the magnetosphere. On the other hand, the fact that fluctuations in the solar wind parameters at a level of only 10% are seen in the simulations to generate a strongly amplified response is probably an even bigger problem for any practical attempts to reach or accurately describe the quiet magnetosphere state.

Declaration of competing interest

The authors declare that they have no known competing financial interests or personal relationships that could have appeared to influence the work reported in this paper.

Acknowledgments

Total current estimates from the Active Magnetosphere and Planetary Electrodynamics Response Experiment (AMPERE) project, PI Brian Anderson, JHU/APL, were downloaded from the project website at http://ampere.jhuapl.edu. We are grateful to the AMPERE team and the AMPERE Science Center for providing the Iridium- derived data products. We acknowledge use of NASA/GSFC's Space Physics Data Facility's CDAWeb service and high-resolution (1 min) OMNI data to provide solar wind and IMF parameters propagated to the sub-solar bowshock. The data was retrieved through the OMNIWeb interface at https://omniweb.gsfc.nasa.gov. SWMF model calculations were conducted by the Community Coordinated Modeling Center at the Goddard Space Flight Center. Simulation results are accessible through their public Runs on Request system (https://ccmc.gsfc.nasa.gov; run IDs: Michael_Hesse_042815_(1-4); Therese_Moretto_061919_1; Therese_Moretto_071019_(1-2)).

References

Akasofu, S., 1981. Energy coupling between the solar wind and the magnetosphere. Space Sci. Rev. 28, 121–190. https://doi.org/10.1007/BF00218810.

Anderson, B.J., Korth, H., Waters, C.L., Green, D.L., Merkin, V.G., Barnes, R.J., Dyrud, L. P., 2014. Development of large-scale birkeland currents determined from the active magnetosphere and planetary electrodynamics response experiment. Geophys. Res. Lett. 41, 3017–3025. https://doi.org/10.1002/2014GL059941.

Anderson, B.J., Korth, H., Welling, D.T., Merkin, V.G., Wiltberger, M.J., Raeder, J., Barnes, R.J., Waters, C.L., Pulkkinen, A.A., Rastaetter, L., 2017. Comparison of predictive estimates of high-latitude electrodynamics with observations of global-scale Birkeland currents. Space Weather 15, 352–373. https://doi.org/10.1002/2016SW001529.

Anderson, B.J., Olson, C.N., Korth, H., Barnes, R.J., Waters, C.L., Vines, S.K., 2018. Temporal and spatial development of global Birkeland currents. J. Geophys. Res. Space Physics 123. https://doi.org/10.1029/2018JA025254.

Borovsky, J. E., 2008. The rudiments of a theory of solar wind/magnetosphere coupling derived from first principles. J. Geophys. Res. 113, 1–14. https://doi.org/10.1029/2007JA012646.

Bhattarai, S.K., Lopez, R.E., Bruntz, R., Lyon, J.G., Wiltberger, M., 2012. Simulation of the polar cap potential during periods with northward interplanetary magnetic field. J. Geophys. Res. 117, A04219. https://doi.org/10.1029/2011JA017143.

Burke, W.J., Kelley, M.C., Sagalyn, R.C., Smiddy, M., Lai, S.T., 1979. Polar cap electric field structures with a northward interplanetary magnetic field. Geophys. Res. Lett. 6, 21–24. https://doi.org/10.1029/GL006i001p00021.

Campbell, W.H., 1989. An introduction to quiet daily geomagnetic fields. Pure Appl. Geophys. 131, 315–331, 1989, doi: 0.1007/BF00876831.

Chisham, G., Lester, M., Milan, S.E., Freeman, M.P., Bristow, W.A., Grocott, A., McWilliams, K.A., Ruohoniemi, J.M., Yeoman, T.K., Dyson, P.L., Greenwald, R.A., Kikuchi, T., Pinnock, M., Rash, J.P.S., Sato, N., Sofko, G.J., Villain, J.-P., Walker, A. D.M., 2007. A decade of the Super Dual Auroral Radar Network (SuperDARN): scientific achievements, new techniques and future directions. Surv. Geophys. 28, 33–109. https://doi.org/10.1007/s10712-007-9017-8.

Clauer, C.R., Friis-Christensen, E., 1988. High-latitude dayside electric fields and currents during strong northward interplanetary magnetic field: observations and model simulation. J. Geophys. Res. 93 (A4), 2749–2757. https://doi.org/10.1029/JA093iA04p02749.

Coroniti, F.V., Kennel, C.F., 1973. Can the ionosphere regulate magnetospheric convection? J. Geophys. Res. 78 (16), 2837–2851. https://doi.org/10.1029/JA078i016p02837.

Coxon, J.C., Milan, S.E., Carter, J.A., Clausen, L.B.N., Anderson, B.J., Korth, H., 2016. Seasonal and diurnal variations in AMPERE observations of the Birkeland currents compared to modeled results. J. Geophys. Res. Space Physics 121, 4027–4040. https://doi.org/10.1002/2015JA022050.

Crooker, N.U., 1992. Reverse convection. J. Geophys. Res. 97 (A12), 19363–19372. https://doi.org/10.1029/92JA01532.

Dods, J., Chapman, S.C., Gjerloev, J.W., 2017. Characterizing the ionospheric current pattern response to southward and northward IMF turnings with dynamical SuperMAG correlation networks. J. Geophys. Res. Space Physics 122, 1883–1902. https://doi.org/10.1002/2016JA023686.

Dungey, J.W., 1961. Interplanetary magnetic field and the auroral zones. Phys. Rev. Lett. 6, 47–48. https://doi.org/10.1103/physrevlett.6.47.

Finlay, C.C., Lesur, V., Thébault, E., et al., 2017. Challenges handling magnetospheric and ionospheric signals in internal geomagnetic field modelling. Space Sci. Rev. 206, 157–189. https://doi.org/10.1007/s11214-016-0285-9.

Fiori, R.A.D., Boteler, D.H., Koustov, A.V., 2012. Response of ionospheric convection to sharp southward IMF turnings inferred from magnetometer and radar data. J. Geophys. Res. 117, A09302. https://doi.org/10.1029/2012JA017755.

Friis-Christensen, E., Kamide, Y., Richmond, A.D., Matsushita, S., 1985. Interplanetary magnetic field control of high-latitude electric fields and currents determined from Greenland Magnetometer Data. J. Geophys. Res. 90 (A2), 1325–1338. https://doi.org/10.1029/JA090iA02p01325.

Gjerloev, J.W., 2012. The SuperMAG data processing technique. J. Geophys. Res. 117, A09213. https://doi.org/10.1029/2012JA017683.

Gonzalez, W.D., 1990. A unified view of solar wind-magnetosphere coupling functions. Planet. Space Sci. 38, 627–631. https://doi.org/10.1016/0032-0633(90)90068-2.

Grocott, A., Milan, S.E., 2014. The influence of IMF clock angle timescales on the morphology of ionospheric convection. J. Geophys. Res. Space Physics 119, 5861–5876. https://doi.org/10.1002/2014JA020136.

Hairston, M.R., Heelis, R.A., 1995. Response time of the polar convection pattern to changes in the north-south direction of the IMF. Geophys. Res. Lett. 22, 631. https://doi.org/10.1029/94GL03385.

Hesse, M., Moretto, T., Kuznetsova, M., Tenfjord, P., Norgren, C., Østgaard, N., Friis-Christensen, E., Opgenoorth, H., 2017. Does the magnetosphere go to sleep?. In: AGU Fall Meeting 2017 abstract #SM13A-2353, available from: adsabs. harvard.edu/abs/2017AGUFMSM13A2353H.

Iijima, T., Potemra, T.A., Zanetti, L.J., Bythrow, P.F., 1984. Large-scale Birkeland currents in the dayside polar region during strongly northward IMF: a new Birkeland current system. J. Geophys. Res. 89 (A9), 7441–7452. https://doi.org/10.1029/JA089iA09p07441.

van de Kamp, M., 2013. Harmonic quiet-day curves as magnetometer baselines for ionospheric current analyses. Geosci. Instrum. Method. Data Syst. 2, 289–304. https://doi.org/10.5194/gi-2-289-2013.

Kauristie, K., Morschhauser, A., Olsen, N., Finlay, C.C., McPherron, R.L., Gjerloev, J.W., Opgenoorth, H.J., 2017. On the usage of geomagnetic indices for data selection in internal field modelling. Space Sci. Rev. 206, 61–90. https://doi.org/10.1007/s11214-016-0301-0.

Klausner, V., Papa, A.R.R., Cândido, C.M.N., Domingues, M.O., Mendes, O., 2016. An alternative way to identify local geomagnetically quiet days: a case study using wavelet analysis. Ann. Geophys. 34, 451–462. https://doi.org/10.5194/angeo-34-451-2016.

Knipp, D.J., Richmond, A.D., Emery, B., Crooker, N.U., de la Beaujardiere, O., Evans, D., Kroehl, H., 1991. Ionospheric convection response to changing IMF direction. Geophys. Res. Lett. 18 (4), 721–724. https://doi.org/10.1029/90GL02592.

Lockwood, M., 2016. Jim Dungey, the open magnetosphere, and space weather. Space Weather 14, 380–383. https://doi.org/10.1002/2016SW001438.

Lu, G., Holzer, T.E., Lummerzheim, D., Ruohoniemi, J.M., Stauning, P., Troshichev, O., Newell, P.T., Brittnacher, M., Parks, G., 2002. Ionospheric response to the interplanetary magnetic field southward turning: fast onset and slow reconfiguration. J. Geophys. Res. 107 (A8) https://doi.org/10.1029/2001JA000324.

McPherron, R.L., Anderson, B.J., Chu, X., 2018. Relation of field-aligned currents measured by the network of Iridium® spacecraft to solar wind and substorms. Geophys. Res. Lett. 45, 2151–2158. https://doi.org/10.1002/2017GL076741.

Milan, S. E., Gosling, J. S., Hubert, B., 2012. Relationship between interplanetary parameters and the magnetopause reconnection rate quantified from observations of the expanding polar cap. J. Geophys. Res. 117, 1–16. https://doi.org/10.1029/2011JA017082.

Milan, S.E., Carter, J.A., Sangha, H., Laundal, K.M., Østgaard, N., Tenfjord, P., et al., 2018. Timescales of dayside and nightside field-aligned current response to changes in solar wind-magnetosphere coupling. J. Geophys. Res. 123 https://doi.org/10.1029/2018JA025645.

Moretto, T., Hesse, M., Vennerstrøm, S., Tenfjord, P., 2018. Estimating the rate of cessation of magnetospheric activity in AMPERE field-aligned currents. Geophys. Res. Lett. 45 (12), 719. https://doi.org/10.1029/2018GL080631, 713– 12.

Murr, D.L., Hughes, W.J., 2001. Reconfiguration timescales of ionospheric convection. Geophys. Res. Lett. 28 (11), 2145–2148. https://doi.org/10.1029/2000GL012765.

Newell, P. T., Sotirelis, T., Liou, K., Meng, C.-I., Rich, F. J., 2007. A nearly universal solar wind-magnetosphere coupling function inferred from 10 magnetospheric state variables. J. Geophys. Res. 112, 1–16. https://doi.org/10.1029/2006JA012015.

Nishida, A., 1968. Coherence of geomagnetic DP 2 fluctuations with interplanetary magnetic variations. J. Geophys. Res. 73 (17), 5549–5559. https://doi.org/10.1029/JA073i017p05549.

Rastätter, L., Hesse, M., Kuznetsova, M., Sigwarth, J.B., Raeder, J., Gombosi, T.I., 2005. Polar cap size during 14–16 July 2000 (Bastille Day) solar coronal mass ejection event: MHD modeling and satellite imager observations. J. Geophys. Res. 110, A07212. https://doi.org/10.1029/2004JA010672.

Richmond, A.D., 2010. On the ionospheric application of Poynting's theorem. J. Geophys. Res. 115, A10311. https://doi.org/10.1029/2010JA015768.

Ridley, A.J., Lu, G., Clauer, C.R., Papitashvili, V.O., 1998. A statistical study of the ionospheric convection response to changing interplanetary magnetic field conditions using the assimilative mapping of ionospheric electrodynamics technique. J. Geophys. Res. 103 (A3), 4023–4039. https://doi.org/10.1029/97JA03328.

Ridley, A.J., 2007. Effects of seasonal changes in the ionospheric conductances on magnetospheric field-aligned currents. Geophys. Res. Lett. 34, L05101. https://doi.org/10.1029/2006GL028444.

Ridley, A.J., Gombosi, T.I., DeZeeuw, D.L., 2004. Ionospheric control of the magnetosphere: conductance. Ann. Geophys. 22, 567–584. https://doi.org/10.5194/angeo-22-567-2004.

Ruohoniemi, J.M., Shepherd, S., Greenwald, R., 2002. The response of the high-latitude ionosphere to IMF variations. J. Atmos. Sol. Terr. Phys. 64, 159–171. https://doi.org/10.1016/S1364-6826(01)00081-5.

Snekvik, K., Østgaard, N., Tenfjord, P., Reistad, J.P., Laundal, K.M., Milan, S.E., Haaland, S.E., 2017. Dayside and nightside magnetic field responses at 780 km altitude to dayside reconnection. J. Geophys. Res. 122, 1670–1689. https://doi.org/10.1002/2016JA023177.

Southwood, D.J., Cowley, S.W.H., Mitton, S. (Eds.), 2015. Magnetospheric Plasma Physics: the Impact of Jim Dungey's Research. Springer, New York. https://doi.org/10.1007/978-3-319-18359-6.

Tenfjord, P., Østgaard, N., 2013. Energy transfer and flow in the solar wind-magnetosphere-ionosphere system: a new coupling function. J. Geophys. Res. 118, 5659–5672. https://doi.org/10.1002/jgra.50545.

Tóth, G., Sokolov, I.V., Gombosi, T.I., Chesney, D.R., Clauer, C.R., et al., 2005. Space Weather Modeling Framework: a new tool for the space science community. J. Geophys. Res. 110 (A12) https://doi.org/10.1029/2005JA011126.

Tóth, G., Holst, B.v. d., Sokolov, I.V., De Zeeuw, D.L., Gombosi, T.I., et al., 2012. Adaptive numerical algorithms in space weather modeling. J. Comput. Phys. 231 (3), 870–903. https://doi.org/10.1016/j.jcp.2011.02.006.

Vennerstrom, S., Moretto, T., Rastätter, L., Raeder, J., 2005. Field-aligned currents during northward interplanetary magnetic field: morphology and causes. J. Geophys. Res. 110, A06205. https://doi.org/10.1029/2004JA010802.

Wygant, J.R., Torbert, R.B., Mozer, F.S., 1983. Comparison of S3-3 polar cap potential drops with the interplanetary magnetic field and models of magnetopause reconnection. J. Geophys. Res. 88 (A7), 5727–5735. https://doi.org/10.1029/JA088iA07p05727.